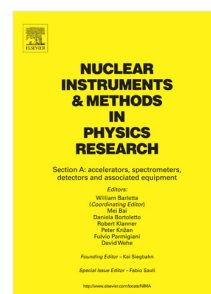


Accepted Manuscript

Density changes in low pressure gas targets for electron scattering experiments

S.N. Santiesteban, S. Alsalmi, D. Meekins, C. Ayerbe Gayoso, J. Bane, S. Barcus, J. Campbell, J. Castellanos, R. Cruz-Torres, H. Dai, T. Hague, F. Hauenstein, D.W. Higinbotham, R.J. Holt, T. Kutz, S. Li, H. Liu, R.E. McClellan, M. Nycz, D. Nguyen, B. Pandey, V. Pandey, A. Schmidt, T. Su, Z. Ye



PII: S0168-9002(19)30865-4
DOI: <https://doi.org/10.1016/j.nima.2019.06.025>
Reference: NIMA 62284

To appear in: *Nuclear Inst. and Methods in Physics Research, A*

Received date: 7 March 2019
Revised date: 12 June 2019
Accepted date: 12 June 2019

Please cite this article as: Density changes in low pressure gas targets for electron scattering experiments, *Nuclear Inst. and Methods in Physics Research, A* (2019), <https://doi.org/10.1016/j.nima.2019.06.025>

This is a PDF file of an unedited manuscript that has been accepted for publication. As a service to our customers we are providing this early version of the manuscript. The manuscript will undergo copyediting, typesetting, and review of the resulting proof before it is published in its final form. Please note that during the production process errors may be discovered which could affect the content, and all legal disclaimers that apply to the journal pertain.

Density Changes in Low Pressure Gas Targets for Electron Scattering Experiments

S. N. Santiesteban^a, S. Alsalmi^b, D. Meekins^c, C. Ayerbe Gayoso^c, J. Bane^d, S. Barcus^e, J. C. Campbell^f, J. Castellanos^g, R. Cruz-Torres^h, H. Daiⁱ, T. Hague^b, F. Hauenstein^j, D. W. Higinbotham^{c,*}, R. J. Holt^{l,k}, T. Kutz^h, S. Li^a, H. Liu^m, R. E. McClellan^c, M. Nycz^b, D. Nguyen^o, B. Pandey^p, V. Pandeyⁱ, A. Schmidt^h, A. Su^b, Z. Ye^l

^aUniversity of New Hampshire, Durham, New Hampshire 03824, USA

^bKent State University, Kent, Ohio 44240, USA

^cJefferson Lab, Newport News, Virginia 23601 USA

^dThe University of Tennessee, Knoxville, Tennessee 37996, USA

^eThe College of William and Mary, Williamsburg, Virginia 23187, USA

^fSaint Mary's University, Halifax, Nova Scotia, Canada

^gFlorida International University, Miami, Florida 33199, USA

^hMassachusetts Institute of Technology, Cambridge, Massachusetts 02139, USA

ⁱCenter for Neutrino Physics, Virginia Tech, Blacksburg, Virginia 24061, USA

^jOld Dominion University, Norfolk, Virginia 23529, USA

^kKellogg Radiation Laboratory, California Institute of Technology, Pasadena, California 91125 USA

^lPhysics Division, Argonne National Laboratory, Argonne, Illinois 60439, USA

^mColumbia University, New York, New York 10027, USA

ⁿStony Brook University, Stony Brook, New York 11794, USA

^oDepartment of Physics, University of Virginia, Charlottesville, Virginia 22904, USA

^pHampton University, Hampton, Virginia 23669, USA

Abstract

A system of modular sealed gas target cells has been developed for use in electron scattering experiments at the Thomas Jefferson National Accelerator Facility (Jefferson Lab). This system was initially developed to complete the MARATHON experiment which required, among other species, tritium as a target material. Thus far, the cells have been loaded with the gas species ^3H , ^3He , ^2H , ^1H and ^{40}Ar and operated in nominal beam currents of up to $22.5\ \mu\text{A}$ in Jefferson Lab's Hall A. While the gas density of the cells at the time of loading is known, the density of each gas varies uniquely when heated by the electron beam. To extract experimental cross sections using these cells, density dependence on beam current of each target fluid must be determined. In this study, data from measurements with several beam currents within the range of 2.5 to $22.5\ \mu\text{A}$ on each target fluid are presented. Additionally, expressions for the beam current dependent fluid density of each target are developed.

Keywords: target, tritium, helium, deuterium, hydrogen, argon

1. Introduction

A modular gas cell target system was developed for use in Jefferson Lab's Hall A for the MARATHON experiment E12-10-103 [1]. The design was specifically developed to safely contain and operate with gaseous tritium. The modular design allows gas cells filled with other species of gas to be installed in the system concurrently. The target was also adapted for experiments E12-11-112 ($x_b > 1$) [2], E12-14-011 ($e, e'p$) [3, 4], E12-17-003 (Hypernuclear) [5] and E12-14-009 (elastic) [6]. MARATHON, together with these experiments, became known as the tritium group of experiments and were performed from December 2017 through November 2018. Prior to the tritium group of experiment operations, a target cell of this same design was filled with argon gas and used by experiment E12-14-012 (Argon) [7, 8] during Spring of 2017.

While the performance of the target was an important consideration, the primary objective of the target system design

and construction was to ensure safe operations with tritium gas under all conditions. These conditions included target cell preparations, loading, storage, transportation, installation, removal, and beam operations. This was accomplished with a modular design, rigorous fabrication and testing, proper quality assurance and quality control, and multiple layers of containment/confinement.

In addition to describing of the target, we present the beam current dependent density of the five gases used with the target system, ^3H , ^3He , ^2H , ^1H and ^{40}Ar . The electron beam deposits energy in the cell end caps as well as in the target fluid. This ionization energy, which is proportional to the beam current, heats the target fluid causing local changes in the density. To determine the magnitude of this effect, data were collected with the left high resolution spectrometer (LHRS) in Jefferson Lab Experimental Hall A during February 2017 for the ^{40}Ar target and December 2017 for the other targets. The beam energy for the study was $2.2\ \text{GeV}$ in all cases. The angle and momentum settings were 17.5° and $1.79\ \text{GeV}$ for ^{40}Ar , and 17.0° and $1.99\ \text{GeV}$ for the other fluids. Analysis shows that a simple quadratic

*Corresponding Author: doug@jlab.org

polynomial function normalized to zero current provides an excellent descriptive fit function for all target fluids.

2. Target System

The modular design allows for multiple cell configurations. It also enables individual cells to be installed in special configurations of the standard Hall A cryogenic target such as the ^{40}Ar target (see Fig. 1). Another feature is that it allows cells to be filled at off-site locations. The tritium cell was filled at Savannah River Site (SRS) by Savannah River Tritium Enterprises (SRTE), with 0.1 grams of tritium gas to a room temperature absolute pressure of 1.38 MPa. It was shipped in a special purpose transport container called the bulk tritium shipping package (BTSP). Including the cell this system provided continuous triple layer confinement throughout the shipping and handling process. This design also allowed the tritium cell to be placed in a storage container in Hall A while normal Hall installation activities were completed. The tritium cell was installed after all other preparatory tasks were completed. The modular sealed gas cell represents a departure from previous designs [9]. Fig. 2 shows the design of the gas cell design. This design is similar to the design proposed in Ref. [10] with engineering details for the construction and loading of these cell in Ref. [11].



Figure 1: A photo of the cell filled with ^{40}Ar installed on the standard Hall A cryogenic target ladder. Below the gas cell the carbon foil targets can be seen which are used to calibrate the reconstruction matrix of the spectrometers.

The configuration of the target system for the tritium experiments is shown in Fig. 3. In this configuration, there are (from top to bottom) four cells loaded with ^3H , ^2H , ^1H , and ^3He as well as a fifth empty cell which was used for background measurements. The cells are contained in a scattering chamber which is under vacuum. The scattering chamber vacuum is isolated from the upstream beam line vacuum by a 0.2 mm thick beryllium window. This window is roughly 30 cm upstream of the target center and is mounted on a reentrant tube that also contains a 15 cm long tungsten collimator with an inner diameter of 12.7 mm. The scattering chamber vacuum, with a pumping system directed to an exhaust stack, provided a second layer of tritium confinement. An exhaust system, (together with strict access controls) capable of maintaining a slight negative pressure in the experimental Hall ensured that the Hall boundary was a third layer of confinement.

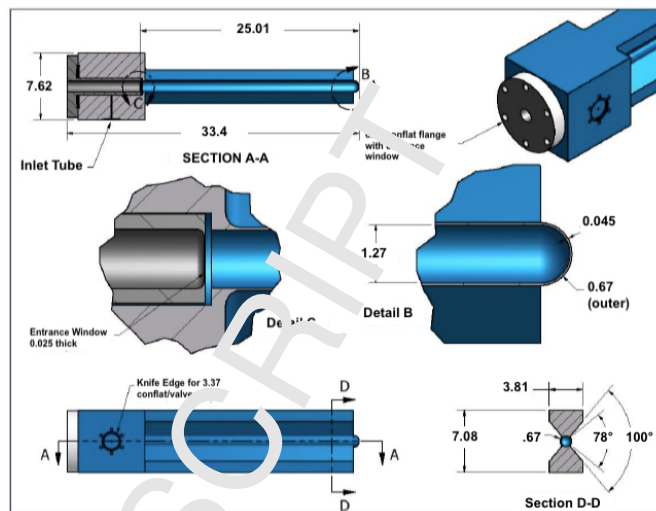


Figure 2: Overview of the design of the gas target cells with the units in cm.

Each cell is machined from ASTM B209 aluminum 7075-T651 plate. Each target cell has a cylindrical fluid space with a length of 25 cm and a diameter of 12.7 mm. The total volume of the cell (including the non-active region) is $33.4 \pm 0.2 \text{ cm}^3$. The thickness of the nearly flat entrance window and hemispherical exit window is nominally 0.25 mm. The parameters at the time of loading for each cell are summarized in Table 1.

Due to machining tolerances, the wall thickness of each cell varies slightly over its length. Thickness measurements were performed for each cell at several locations as schematically represented in Fig. 4 and summarized in Table 2. These measurements were performed with a Magna Mike 8600 Hall effect thickness gauge which provides a relative uncertainty of 0.001 mm and an absolute uncertainty of 0.007 mm. The error shown in the Table 2 indicates the standard deviation of multiple measurements in a 2 mm radius for a given location. The ^{40}Ar cell, installed in February 2017, was later evacuated and installed as the empty cell for the tritium group of experiments, so Table 2 shows the ^{40}Ar and the empty cell in a single column.

Once installed in the Hall A scattering chamber, the target cells were cooled to 40 K with the temperature maintained using a 15 K helium supply and a controlled heater. This cooling was required to remove the modest amount of heat generated by the electron beam passing through the target fluid, cell entrance and cell exit, which, in total, was about 15 W. To ensure cell integrity, the maximum beam current permitted on any of the cells was $22.5 \mu\text{A}$ [11]. The heat generated by the tritium decay is very small, about 50 mW.

3. Hall A Spectrometers

The data were acquired with the left high resolution spectrometer (LHRS). For a detailed description of the LHRS see Ref. [12]. The basic components of the LHRS are a normal conducting quadrupole (Q1), a superconducting quadrupole (Q2), a superconducting dipole (D), and a superconducting quadrupole



Figure 3: Ladder assembly showing the five cells that were installed for the MARATHON experiment, ^3H , ^2H , ^1H , ^3He and empty cell from top to bottom, as assembled during Fall 2017 to Spring 2018 run period.

Target	Fill Pressure (kPa)	Fill Temp (K)	Thickness (mg/cm ²)
^{40}Ar	3447	291.0	1455 ± 6
^3H 1 st	1400	296.3	85.1 ± 0.8
^3H 2 nd	1393	293.8	84.8 ± 0.7
^3He	1772	294.3	53.4 ± 0.6
^2H	3549	296.1	102.2 ± 0.8
^1H	3549	297.4	70.8 ± 0.7

Table 1: The target thickness in gm/cm² for each of the gas cells based on the fill pressures and temperatures. Temperatures have an uncertainty of 0.1 K.

(Q3) in a Q-Q-D-Q configuration. The quadrupoles focus scattered charged particles while the dipole bends these particles, within a given momentum range, to the detectors. After passing through the spectrometer magnets, the scattered particles pass through two vertical drift chambers (VDCs) that provide tracking information [13]. Two layers of scintillator hodoscopes, s0 and s2, are on either side of a gas Cherenkov detector filled with CO₂ [14]. The hodoscopes provide trigger and time of flight for the detected particles. The Cherenkov provides identification of electrons with approximately 99% efficiency and reject π^- below a momentum of 4.8 GeV/c. The last element in the detector stack is the shower calorimeter. Electrons passing through the calorimeter lead glass blocks induce a cascade of pair production and bremsstrahlung radiation from which their energy can be determined [12].

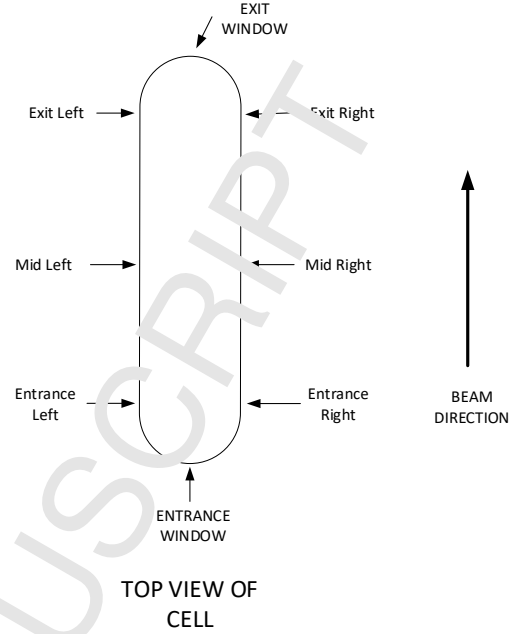


Figure 4: Measurement locations of the cells represented schematically.

4. Beam Current Monitor

The beam current monitor (BCM) is a system of three independent devices and a current source [15]. This is a dedicated system in Hall A and while independent of the target effects, this system is the dominant source of systematic uncertainty in the current dependent density studies presented herein. The BCM system consists of a toroidal sensor (Unser) [16], located between upstream and downstream RF cavities, and a data-acquisition system. A current source, which is connected to a wire which passes through the Unser, is used to calibrate the Unser immediately prior to each use of the device and the Unser is then used to calibrate the BCMs with the electron beam.

The Unser monitor is composed of two identical toroidal coils driven in opposite directions by an external source. The DC component of the current flowing through the toroid sensor is detected by a magnetic modulator. The beam current passing through the cores produces a flux imbalance, which generates an output signal proportional to the even harmonics of the frequency of excitation. In the absence of a DC current, the sum of the signals is zero [15].

The temperature controlled Unser has a sensitivity to beam current of about 4 mV/ μA and has a DC offset subtracted stability within 0.1% [15]. The systems DC offset does slowly drift, necessitating the current calibration to be done immediately prior to using it for an absolute current calibration of the RF cavities. Once calibrated, the RF cavities are used to continuously monitor the beam current. The calibrations are checked periodically throughout the course of an experiment. To put the signals from the Unser and RF cavities into the scalars of Hall's fast data acquisition system, a voltage to frequency (V/F) converter is used along with a discriminator. Figure 5 shows the Unser calibration with a known DC current source, the response

Location	⁴⁰ Ar/Empty Cell Thickness (mm)	³ H Cell Thickness (mm)	¹ H Cell Thickness (mm)	² H Cell Thickness (mm)	³ He Cell Thickness (mm)
Entrance	0.254 ± 0.005	0.253 ± 0.004	0.311 ± 0.001	0.215 ± 0.004	0.203 ± 0.007
Exit	0.279 ± 0.005	0.343 ± 0.047	0.330 ± 0.063	0.294 ± 0.056	0.328 ± 0.041
Exit left	0.406 ± 0.005	0.379 ± 0.007	0.240 ± 0.019	0.422 ± 0.003	0.438 ± 0.010
Exit right	0.421 ± 0.005	0.406 ± 0.004	0.519 ± 0.009	0.361 ± 0.012	0.385 ± 0.016
Mid left	0.457 ± 0.005	0.435 ± 0.001	0.374 ± 0.004	0.447 ± 0.009	0.487 ± 0.060
Mid right	0.432 ± 0.005	0.447 ± 0.004	0.503 ± 0.005	0.371 ± 0.012	0.478 ± 0.007
Entrance left	0.508 ± 0.005	0.473 ± 0.003	0.456 ± 0.010	0.442 ± 0.005	0.504 ± 0.003
Entrance right	0.424 ± 0.005	0.425 ± 0.003	0.457 ± 0.006	0.372 ± 0.011	0.477 ± 0.011

Table 2: Cell wall thickness measurements for different cells as measured by a Hall effect thickness gauge.

of the system is found to be $(249.7 \pm 9.6) \times 10^{-6} \mu\text{A/Hz}$.

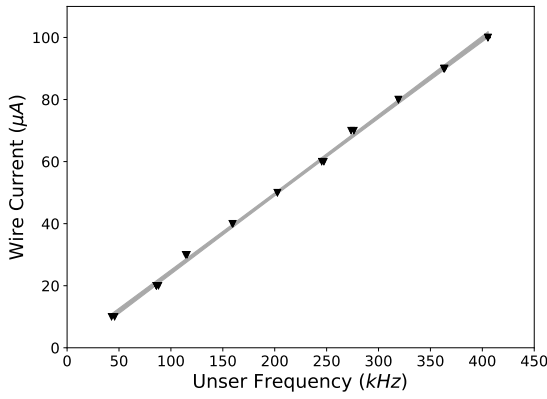


Figure 5: Wire Unser calibration. The band represents the 95% confidence level of the linear fit.

The beam current monitors (BCM) are 1497 MHz resonant cavities located immediately before and after the Unser and are used to continuously monitor the beam currents in Hall A (see Fig. 6). The cavities are composed of loop antennas located where the magnetic field is maximum. When the beam passes through, the output RF signal is proportional to the current [15]. As consequence, the BCM response is linear with respect to the current. Like the Unser, the signals from the RF cavities are filtered by a V/F converter. Several values of beam current (measured by the calibrated Unser) are used to determine the linear dependence of the BCM as shown in Fig. 7. In general, the beam current can be then calculated using

$$I = g_{\text{BCM}} \cdot f + O, \quad (1)$$

where g_{BCM} and O are the fit parameters, which correspond to $(326.4 \pm 1.4) \times 10^{-6} \mu\text{A/Hz}$ and $0.1 \pm 0.09 \mu\text{A}$, respectively. Finally, for any given beam induced frequency f , the current I is given by Eq. 1. Unfortunately the BCM system becomes much less accurate for beam currents below $\sim 5 \mu\text{A}$.

5. Method Overview

The density of the target is well known when loaded but experience and simulations have shown that the beam current will

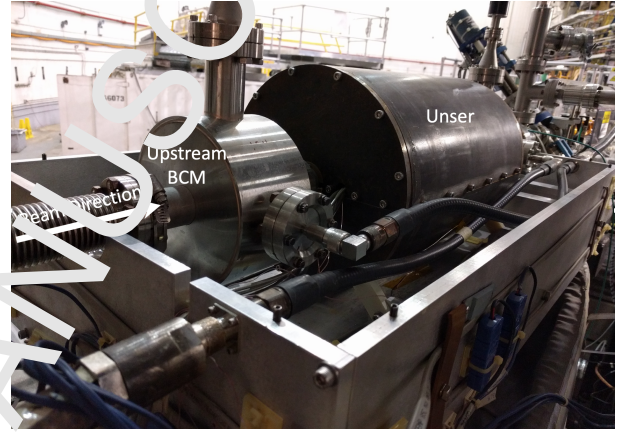


Figure 6: Shown is the upstream beam current monitor (BCM) and the Unser cavity as installed in the Hall A beamline. The thermal insulating cover, that keeps the systems at a stable temperature, has removed for the photo.

decrease the local density of the target fluid in the beam path. The magnitude of this effect depends on the beam current and target fluid species and must be quantified to accurately determine cross sections, ratios and other comparisons of data collected with the multiple gas cells [17]. It was shown (with the exception of the argon cell) that the target density reaches equilibrium within a few seconds from when the electron beam first impinges on the cell and the density was constant with stable beam current. The purpose of these measurements and analysis is to develop a calibration of the target density as a function of beam current for each gas species.

In order to extract the current dependent density correction, the LHRS is used to measure the event rate for several beam currents. The normalized yield is determined by applications of corrections to the raw event rate. These corrections include: integrated charge during the measurement, particle identification, acceptance cuts, detector efficiencies, and live times. The normalized yield Y_{norm} is then given by

$$Y_{\text{norm}} = \frac{PS \cdot N}{Q \cdot \epsilon \cdot LT}, \quad (2)$$

where N is the number of good electrons, PS is the prescale factor of the DAQ system, Q is the integrated charge, and ϵ is the combined efficiency of the detectors, triggers and events selection cuts and LT is the live-time. Each one of these parameters

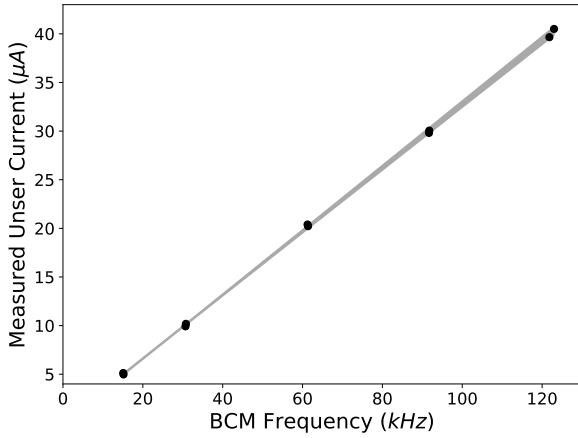


Figure 7: BCM calibration data shown with the 95% confidence level from a linear regression.

is explained in detail in the following sections.

5.1. Event Selection

To improve counting efficiency and maximize live time, a compound trigger was used. This trigger required both scintillator planes and the Cherenkov detector to have signals above threshold in order to exclude π^- events. To extract a good electron sample, several cuts were applied to the data. These cuts can be summarized in two groups: acceptance cuts, which ensure that the events are selected within an acceptable spectrometer phase space, and tracking/particle identification (PID) cuts, which focus on the selection of electrons scattered from the target fluid. These selection cuts are:

- Momentum and angular acceptance cuts: Specifically, the ranges used to determine Y_{norm} are $|\delta p/p| < 4.5\%$, $|\theta - \theta_0| < 30$ mrad and $|\phi| < 25$ mrad
- Target length cut: This cut excludes events reconstructed back to the target windows and reduced background by limiting the effective target length $|z_{\text{eff}}| < 8$ cm
- Only events with a single track in the VDC were kept
- A particle ID cut was applied to the Cherenkov ADC sum
- A particle ID cut was applied to the shower calorimeter

With these particle selection cuts, we found that the results remained stable within 1% run to run. The cut for the reaction vertex was chosen such that the contamination from the aluminum end-caps was smaller than 2%. The systematic effects of the aluminum background events were studied for all the targets are included in the systematic uncertainties.

5.2. Estimation of Efficiencies

A number of efficiencies were applied to the data to produce Y_{norm} . For simplicity, in this analysis only electron events with

one track in the VDC were selected. The ratio between the total number of electron events with one track and the total number of triggered electrons (including multi-track and non-track particles) defines the VDC efficiency.

The trigger efficiency was calculated using another trigger type, where only both scintillators were required to record the events. In this sense, the difference between the main trigger and the efficiency trigger is the Cherenkov detector. The ratio between the events recorded with the main and the efficiency trigger corresponds to the trigger efficiency.

The Cherenkov efficiency was calculated by selecting a sample of electrons detected in the calorimeter and determining the number of events that also were detected in the Cherenkov detector. The calorimeter efficiency was measured by selecting a sample of electrons in the Cherenkov detector and counting the number of these electrons that also fired the calorimeter.

For these measurements, the trigger, Cherenkov, and calorimeter efficiencies were $> 99\%$. The tracking efficiency was dependent on the absolute rate in the LHRS and varied for 97 to 99%.

5.3. Live Time Calculation

The live-time is related with the limitation of the speed of data acquisition system (DAQ) to record events. It depends on the electronics, computers and trigger rate and is calculated using the ratio of the number of events recorded over the total number of events seen by the trigger. Typical values for the live-time ranged 93-97% depending the trigger rate in the left LHRS as well as the DAQ prescale setting.

5.4. Total Charge

The beam is not completely stable throughout the run; it may trip off or fluctuate over time. Therefore, we obtained the calibration data when the beam was mostly stable, and only runs where the average current is within a window of $\pm 2 \mu\text{A}$ of the requested current are used. The charge is calculated by integrating the current over time using the BCM calibration result (see Section 4).

6. Solid Target Check

The aim of the analysis is to measure the density change when the beam is on the gas targets using the yield analysis. In order to test the method, the same analysis is applied to a solid target. The ^{40}Ar experiment used a carbon foil while for the Tritium experiments used an aluminum target. Unlike the fluid targets, the solid target density is not measurably affected by the beam current.

Figure 8 shows Y_{norm} for the solid aluminum target which was calculated using Eq. 2 for different beam currents. It was normalized with respect to the lowest current yield value. The plot shows that Y_{norm} did not change to within about 0.5% at the 95% confidence level which is well within the uncertainty of the measurement.

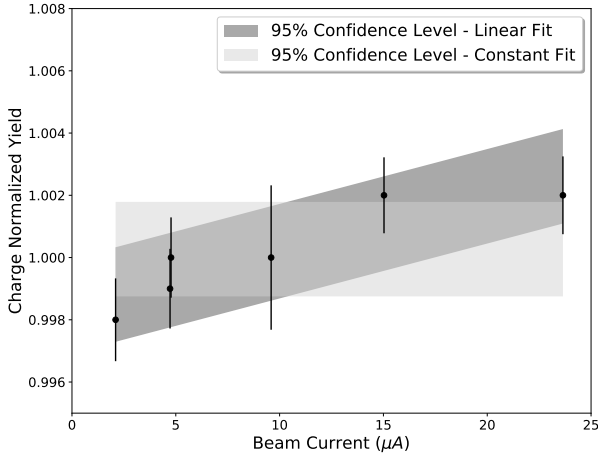


Figure 8: Shown is the normalized yield vs. beam current the aluminum solid target used during the tritium group experiments. Shown are the 95% confidence level bands for a constant and for a linear regression of the data. These results are consistent with an ability to determine density changes with our experimental setup to approximately 0.5% at the 95% confidence level.

7. Background Contamination

The aluminum windows of the target cell contribute a background to the measured raw yield for each of the gas targets. To measure this background (henceforth referred to as contamination) in the case of the ^{40}Ar experiment, a dummy target with aluminum foils with total thickness matching the radiation length of the argon filled cell was used. In the case of the tritium experiments, an empty cell (or dummy cell) was used. The normalized yields from these targets were then subtracted from the applicable Y_{norm} . To check the current dependence of this subtraction, a comparison between the background at low and high current was measured for the dummy/empty targets. The charge yield given by Eq. 1 was binned in y_{pr} segments along the target length, and the ratio of the event at high current to low current was determined. The ratio was found to be 1.006, which indicates that the background subtraction is independent of current, as expected.

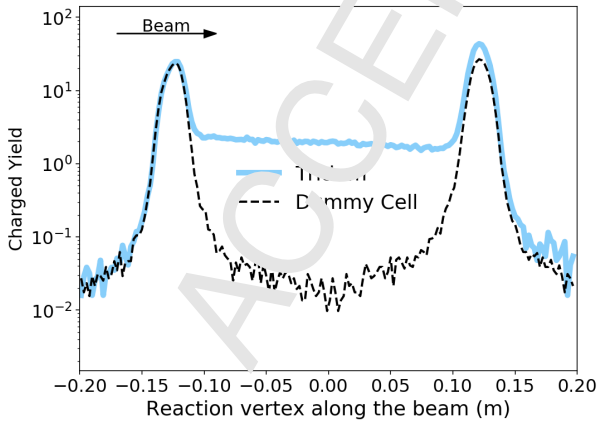


Figure 9: Background contamination spectrum of the dummy target compared with that of tritium at 2.5 μA . Both spectra are normalized.

Figure 9 shows the spectra of the charge normalized yield for the empty (or dummy) cell and the tritium gas, for a beam current of 2.5 μA . To optimize the signal to background ratio, events contributing to the Y_{norm} were selected from a symmetric region of ± 8 cm about the center of the target. Therefore, the contamination fraction is the ratio of Y_{norm} for the empty cell to Y_{norm} for the gas cell of interest. Table 3 summarizes the percentage of background contamination found in the gas targets for each beam current used in the study.

Current (μA)	^3H (%)	^4He (%)	^{12}C (%)	^1H (%)	Current (μA)	Argon (%)
2.5	1.7	1.6	0.7	1.1	2.5	0.3
5	1.7	1.6	0.7	1.2	4.5	0.3
10	1.7	1.7	0.8	1.2	8	0.3
15	1.8	1.8	0.8	1.3	12	0.3
22.5	1.8	1.8	0.8	1.3	15	0.3
					18	0.3

Table 3: Aluminum window contamination in a ± 8 cm range with respect to the center of the target at each nominal current. Note that these currents were not the same for both experiments.

8. Gas Target Results

The density correction was determined for each gas species by measuring Y_{norm} as a function of beam current I_{beam} . The function is then normalized to 1 for $I_{\text{beam}} = 0$. The density each gas cell for zero beam current is the same as that of the load density. Figures 10, 11a, 11b, 11c and 11d show the density correction for the different gas targets. It is easily seen that the density decreases with the current and that the behavior of the density correction factor f is modeled well by a quadratic function

$$f(I_{\text{beam}}) = a \cdot I_{\text{beam}}^2 + b \cdot I_{\text{beam}} + c, \quad (3)$$

where a , b and c are the fit parameters. Table 4 shows the fit parameters for each gas species. The density correction factor $f(I_{\text{beam}})$ is determined for each gas by substitution of these parameters in Eq. 3. The density correction factor determined in this manner is valid for the current range 0 – 22.5 μA . The error bar in the plots represents the statistical uncertainty only, and a fit was calculated with respect to those values with a 95% confidence band in blue. The gray hatched 95% confidence band represents a fit including both statistical and systematic uncertainties. Since many data analyses require ratios of different targets, we also provide the ratio of the density changes, shown in Fig. 12.

8.1. Systematic Uncertainties

Several corrections are applied to the data in this analysis, and since the current is different for every point, the uncertainties are evaluated at every point. Confidence bands for each fit including the systematic uncertainties are shown in Fig. 10, 11a, 11b, 11c and 11d. They include the uncertainty in the charge, live-time and detector efficiencies.

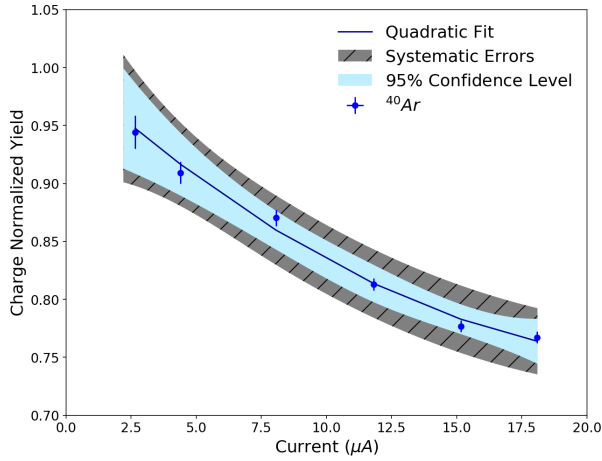


Figure 10: Shown is the ^{40}Ar target's local density as a function of beam current.

The BCM monitors are effective over a range from 0 to 100 μA . However, low current measurements have a slightly higher uncertainty causing the uncertainty in the charge to be current dependent. The uncertainty in the current and charge is estimated using the BCM calibration shown in Fig. 7, together with the error covariance matrix. This is the dominant source of systematic uncertainty in the determination of the density reduction factor $f(I_{\text{beam}})$.

The background contamination coming from the entrance and exit windows is also a source of systematic uncertainty. This is due to the thickness variations in the cell entrance and exit windows which can be seen in Figure 9. Therefore, in order to calculate the background uncertainty in the measurement, the percentage of background was calculated in y_{tar} for the values of ± 4 cm, ± 7 cm and ± 10 cm from the center of the target. The same normalization procedure was followed for each of the different cuts in the reaction vertex region to calculate $f(I_{\text{beam}})$. Finally, the uncertainty in the background contamination is given by the standard deviation of the average of multiple $f(I_{\text{beam}})$ obtained with the different cuts. The standard deviation was never more than 1% for each current.

Furthermore, 1% systematic uncertainties were estimated for the live-time, VDC one-track efficiency, trigger efficiency, detector and cut efficiencies of the gas Cherenkov and π^- rejection.

9. Summary

A novel design for low density gas targets has been used in the Jefferson Lab electron beam with a number of different gas species. These cells have proven to be extremely robust and satisfied the safety requirements necessary for holding 1 kCi of tritium gas. In this manuscript, we have shown how the local density of these cells changes when an electron beam passes through them. The 5% to 10% changes that were measured at 22.5 μA for the different gas species are consistent with the design expectations. Determination these density changes was

^3H Fit Parameters		^3H Correlation Factors	
a	$(1.06 \pm 0.36) \times 10^{-4}$	C(a, b)	-0.974
b	$(-6.8 \pm 0.89) \times 10^{-3}$	C(b, c)	-0.888
c	$1. \pm 0.003$	C(a, c)	0.801
^3He Fit Parameters		^3He Correlation Factors	
a	$(1.04 \pm 0.25) \times 10^{-4}$	C(a, b)	-0.973
b	$(-5.1 \pm 0.64) \times 10^{-3}$	C(b, c)	-0.879
c	1 ± 0.003	C(a, c)	0.779
^2H Fit Parameters		^2H Correlation Factors	
a	$(1.16 \pm 0.29) \times 10^{-4}$	C(a, b)	-0.973
b	$(-6.7 \pm 0.71) \times 10^{-3}$	C(b, c)	-0.895
c	$1. \pm 0.003$	C(a, c)	0.805
^1H Fit Parameters		^1H Correlation Factors	
a	$(1.70 \pm 0.7) \times 10^{-4}$	C(a, b)	-0.978
b	$(-9 \pm 0.12) \times 10^{-3}$	C(b, c)	-0.881
c	$1. \pm 0.003$	C(a, c)	0.788
^{40}Ar Fit Parameters		^{40}Ar Correlation Factors	
a	$(4.5 \pm 1.5) \times 10^{-4}$	C(a, b)	-0.981
b	$(-2.1 \pm 0.3) \times 10^{-2}$	C(b, c)	-0.942
c	$1. \pm 0.02$	C(a, c)	0.867

Table 4: Fit parameters obtained for the percentage of density change calculation with respect to the beam current.

critical for experiments using these cells for cross section measurements.

10. Acknowledgments

We wish to thank the staff of the Thomas Jefferson National Accelerator Facility for their help safely installing and removing the tritium cells. We also acknowledge the critical efforts of Savannah River Site and Savannah River Tritium Enterprises. And special thank to Marcy Stutzman for proofreading this manuscript. This work was supported by the U.S. Department of Energy (DOE) contract DE-AC05-06OR23177 under which Jefferson Science Associates operates the Thomas Jefferson National Accelerator Facility, DOE contract DE-AC02-06CH11357, DOE contract DE-SC0013615, and by National Science Foundation (NSF) Grant No. NSF PHY 1506459.

References

- [1] G. Petratos, et al., JLab Experiment E12-10-103 (2010).
- [2] P. Solvignon, et al., JLab Experiment E12-11-112 (2011).
- [3] O. Hen, L. B. Weinstein, S. Gilad, W. Boeglin, et al., JLab Experiment E12-14-011 (2013).
- [4] R. Cruz-Torres, et al., Comparing proton momentum distributions in $A = 3$ nuclei via ^3He and $^3\text{H}(e, e' p)$ measurements (2019). arXiv:1902.06358.
- [5] L. Tang, F. Garibaldi, P. E. C. Markowitz, S. N. Nakamura, J. Reinhold, G. M. Urciuoli, JLab Experiment E12-17-003 (2017).
- [6] L. S. Myers, D. W. Higinbotham, J. R. Arrington, JLab Experiment E12-14-009 (2014). arXiv:1408.5283.
- [7] O. Benhar, et al., JLab Experiment E12-14-012 (2014). arXiv:1406.4080.
- [8] H. Dai, et al., First Measurement of the $\text{Ar}(e, e')X$ Cross Section at Jefferson Lab, Phys. Rev. C 99 (2019) 054608.
- [9] D. Beck, et al., A Cryogenic tritium target system for nuclear physics experiments, Nucl. Instrum. Meth. A277 (1989) 323–337.

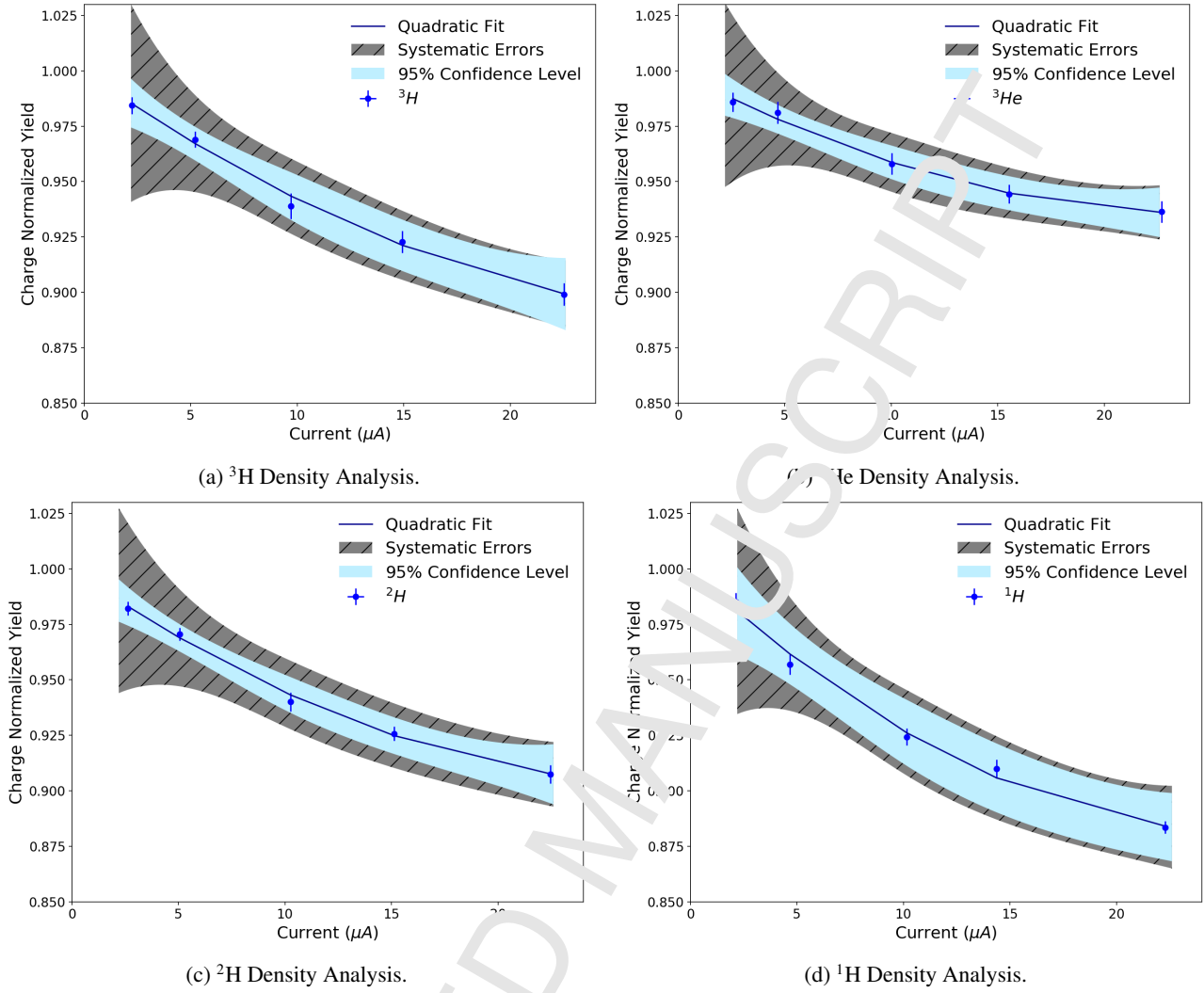


Figure 11: Shown is local density of the ^3H , ^3He , ^2H and ^1H targets as a function of beam current.

- [10] B. Brajuskovic, T. O'Connor, R. J. Holt, J. Reneker, D. Meekin, P. Solvignon, Thermomechanical design of a static gas target for electron accelerators, Nucl. Instrum. Meth. A729 (2013) 469–473.
- [11] D. Meekins, et al., Cryogenic Tritium Gas Target for Electron Scattering Experiments, in preparation for Nucl. Instrum. and Meth. A.
- [12] J. Alcorn, et al., Basic Instrumentation for Hall A at Jefferson Lab, Nucl. Instrum. Meth. A522 (2004) 294–300.
- [13] K. G. Fissum, et al., Vertical drift chamber for the Hall A high-resolution spectrometers at Jefferson Lab, Nucl. Instrum. Meth. A474 (2001) 108–131.
- [14] M. Iodice, et al., The CO-2 gas Cherenkov detectors for the Jefferson Lab Hall-A spectrometers, Nucl. Instrum. Meth. A411 (1998) 223–237.
- [15] J. Denard, A. Saha, G. L. Vessiere, High Accuracy Beam Current Monitor System for CEBAF's Experimental Hall A, Conf. Proc. C0106181 (2001) 2326–2328.
- [16] K. B. Unser, The Parametric current transformer: A Beam current monitor developed for LEP, IP Conf. Proc. 252 (1992) 266–275.
- [17] R. Holt, W. Korsch, D. Meekins, T. O. Connor, G. Petratos, R. Ransome, P. Solvignon, B. Wojtsek, A Tritium Gas Target for Jefferson Lab (2015).

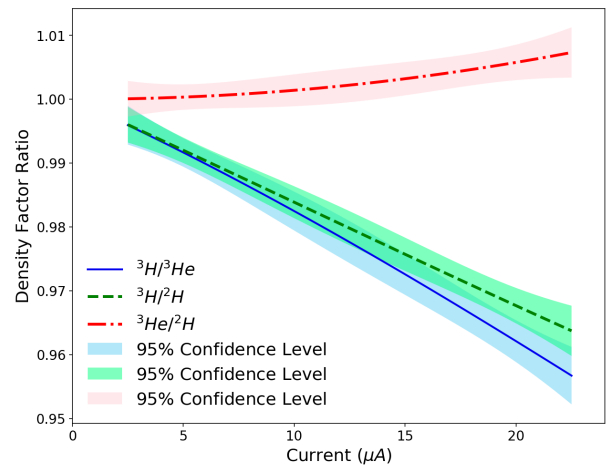


Figure 12: For experiments that will be taking the ratios between different targets, we also determined the ratio the density changes. As some of the systematic affects cancel in the ratio, these uncertainties are slightly smaller than the absolute density change determinations.